



ELSEVIER

Contents lists available at ScienceDirect

Measurement

journal homepage: www.elsevier.com/locate/measurement

Review

Thermal error analysis in precision length measurements

A. Jakstas^{a,*}, S. Kausinis^b, R. Barauskas^c, A. Kasparaitis^d, A. Barakauskas^e^a Department of Engineering Mechanics, Kaunas University of Technology, K. Donelaicio 73, LT-44244 Kaunas, Lithuania^b Department of Engineering Mechanics, Kaunas University of Technology, A. Mickeviciaus 37, LT-44244 Kaunas, Lithuania^c Department of System Analysis, Kaunas University of Technology Studentu 50-407, LT-51368 Kaunas, Lithuania^d Department of Machine Engineering, Vilnius Gediminas Technical University, J. Basanaviciaus g. 28, LT-03224 Vilnius, Lithuania^e Precizika-Metrology, Zirmunu g. 139, LT-09120 Vilnius, Lithuania

ARTICLE INFO

Article history:

Received 19 November 2013

Received in revised form 16 January 2014

Accepted 29 January 2014

Available online 7 February 2014

Keywords:

Thermal error analysis

FE modelling

Line scale comparator

ABSTRACT

One of the most significant factors which determine the precision of a machine is elastic thermal deformations of the structural components. The paper describes the practical application of thermal error analysis that aims towards the reduction of thermally-induced errors for precision length measurement systems operating in non-ideal environments. Finite element analysis and experimental investigations were carried out to examine the core thermal processes and to demonstrate the existence and feasibility of the thermal modal analysis in precision line scale calibration system.

© 2014 Elsevier Ltd. All rights reserved.

Contents

1. Introduction	133
2. Thermal error analysis techniques	134
3. FE modelling for investigation of structural components	134
4. Experimental setup	138
5. Thermal error measurement	142
6. Conclusions	145
References	146

1. Introduction

The thermo-elastic behaviour of a precision machine is one of the most important factors in determining its accuracy capability. With the improvement of machine accuracy, errors induced by thermo-elastic deformations due to internal and external heat sources become even more significant.

This issue is particularly relevant to the length measurement in non-ideal application environments, under the influence of many external factors that are not part of the desired measurement, namely, that are affected by a wide spectrum of seismic excitations, non-homogeneous temperature fields, electro-magnetic noise and other disturbances. Thermal effects here are still one of the largest sources of dimensional errors and apparent non-repeatability of measurement [1,2].

Nevertheless, compensation of machine tools should always deal with geometrical errors changing as a result of thermal changes and load effects. Thermal and

* Corresponding author. Tel./fax: +370 37 323855.

E-mail address: aurimas.jakstas@ktu.lt (A. Jakstas).

mechanical stiffness therefore remains a primary design criterion for high precision machines.

Although a lot of attention in the world has been paid to research of precision length calibration problems, the creation of new components and systems, and elevation of existing ones with the aim to meet the fast-growing scientific and industrial needs, many specific problems have been left unsolved. Precision systems often are too complex and different, so it is complicated or almost impossible to transfer and adapt the findings of such research directly for system perfection.

2. Thermal error analysis techniques

The numerous approaches and techniques to the assessment of thermo-elastic behaviour of precision machines have been systematically developed and reported over several decades. Significant work towards understanding and subsequent reducing of thermally induced errors was done in the CNC and CMM's arena [3].

Thermal error analysis techniques include series of passive to active methods to increase the thermal stability of a machine. These cover reducing the system sensitivity to the heat flow by structural design, management of the heat sources, control of the machine environment, and compensation for measured deviations.

A comprehensive review of the work carried out over the last decade in the estimation and compensation of temperature dependent errors in machine tools has been done in [1]. A generalised approach has been analysed that was proposed by many researchers towards handling the problem of non-uniform temperatures in the machine tools. The techniques in modelling the thermal behaviour have been considered, namely finite element analysis, coordinate transformation methods, and neural networks. The methods of measurement of the temperature and error components and correction of these errors in real-time have been described in [1].

An effort to develop a systematic methodology to improve the accuracy of a machine tools by applying the thermal modal analysis has been presented in [4]. The analysis was exploited for the temperature sensor placement strategy and thermal error modelling. Finite element analysis (FEA) is utilised to examine the essence of thermal process of machine tool elements. Numerical simulation and practical experiments are carried out to illustrate the existence and feasibility of the thermal modal analysis in reality [5–7].

In the aforementioned studies the numerous approaches and solutions have been considered to control the generation and flow of heat in precision machines. Although a lot of attention has been paid to research and develop a compensation strategies for thermal errors, many specific problems have been left unsolved. Precision systems often are too complex and different, so it is complicated or almost impossible to transfer and adapt the findings of such research forthrightly for the creation of new components and systems, and elevation of existing ones. New research activities and advanced modelling and simulation are still of

relevance in order to provide “advisory service” for system perfection.

The paper describes the error-related problems specific to line scale calibration that are caused primarily by thermal deviations of the comparator components and the scale.

3. FE modelling for investigation of structural components

The structural components of the precision line scale comparator consist of four main parts, namely the body of the machine, a laser interferometer, a translating system and a detecting apparatus. The body of the machine, which is made of granite surface plate, is used as the base of the machine and as a guide for the moving carriage. Measurement of the displacement of the carriage is realised by laser interferometer that consist of Zygo ZMI 2000 laser head and interferometer with the single-pass arrangement. The interferometer provides a resolution of 0.62 nm [10].

The comparator is developed to calibrate line graduation scales and incremental linear encoders. A moving CCD microscope serves as structure localisation sensor for the measurements of line scales. The angular control loop – together with the numerical procedure – has been applied to compensate and reduce the Abbe uncertainty contribution. The comparator was designed to achieve expanded measurement uncertainties ($k = 2$) down to 7×10^{-7} m ($L = 1$ m) in dynamic regime. It enabled to trace the calibration of line scale of up to $L \leq 3.5$ m long to the wavelength standard. The magnification and numerical aperture of the NIKON objective lens used is 20 \times and 0.4 respectively. The microscope on the carriage guided on aerostatic bearings is moved with a controlled velocity of 1–10 mm/s.

Microscopes are now used for a wide variety of tasks in addition to imaging, requiring complex laser optics, metrology tools, and precision motion mechanisms in conjunction with the basic microscope structure.

Structural designs of current microscopes, which have retained similar cantilevered shapes for decades, make such advanced setups cumbersome and sensitive to thermal and mechanical disturbances. The mechanical performance of the microscope has become the limiting factor in particular for many high-resolution experiments.

Inhomogeneous thermal expansion of the body of the microscope is a major cause of instability during experiments. However, the optical train of the infinity-corrected microscope is not sensitive to motion in all directions. By using symmetry, the expansion of the mechanical structure can be channeled into directions which do not effect the optical measurement [8,9].

One of precarious temperature disturbances is the heat spread out by the CCD camera of the measuring microscope. As the steady-state temperature under the operating conditions is known, the thermal expansion process can be modelled by using the FE simulation, and the temperature values can be found at all points of the microscope structure. Having the temperature values

obtained, the displacements due to thermal expansion can be calculated at any point of the structure.

The processes can be analysed by performing the thermal analysis of the comparator structure by using the FE computational models based on the well-known partial differential equations, (PDE), and its boundary conditions as

$$\lambda \left(\frac{\partial^2 T}{\partial x^2} + \frac{\partial^2 T}{\partial y^2} + \frac{\partial^2 T}{\partial z^2} \right) + b(x, y, z) = \rho c \frac{\partial T}{\partial t} \in V$$

$$\lambda \left(n_x \frac{\partial T}{\partial x} + n_y \frac{\partial T}{\partial y} + n_z \frac{\partial T}{\partial z} \right) + q + \alpha(T - T_\infty(x, y, z)) = 0 \in S_q$$

$$T - \tilde{T} = 0 \in S_T \tag{1}$$

where $T(x, y, z)$ is the temperature at a point, λ , ρ and c are the heat conductivity coefficient (W/m K), the mass density (kg/m³) and the specific heat (J/m³ K) correspondingly; $b(x, y, z)$ is the body power generated at a point (W/m³). $b(x, y, z)$ is employed in order to describe the heat powers (if any) generated within the structure, such as in space occupied by certain electronic equipment, which is not presented in detail within the FE model. The Cauchy boundary condition on surface S_q enables to determine the heat flux density flowing through the surface of the structure due to externally applied known surface heat flux

density q (W/m²) and due to convective heat exchange between the solid structure and the surrounding air $\alpha(T - T_\infty)$, where α is the convection coefficient q (W/m² K), and T_∞ is the temperature of the surrounding air at point (x, y, z) of surface S_q . Term $\alpha(T - T_\infty)$ is the most important term, the proper definition of which influences significantly heavily the heat power exchange through the surface of the structure. It is defined over all zones of the surface, which have contact with the air. On the contrary, term q is used rarely. Although the term may present a rough estimation of the heat flux density supplied to the structure from external sources, the Dirichlet boundary condition over surface S_T is mostly preferred. It enables to define the estimation of the thermal situation on the boundary in terms of prescribed temperature \tilde{T} .

The approximation of Eq. (1) over a finite element and the application of the weighted residual approach enables to present the thermal analysis problem in the form of the structural heat conductivity equation as

$$[C]\{\dot{T}\} + [K_{Th}]\{T\} = \{S_\infty\} \tag{2}$$

where $[C]$ and $[K_{Th}]$ are matrices of heat capacity and heat conductivity, $\{S_\infty\}$ – nodal vector of heat sources of the element determined by the heat exchange over the surface of the body.

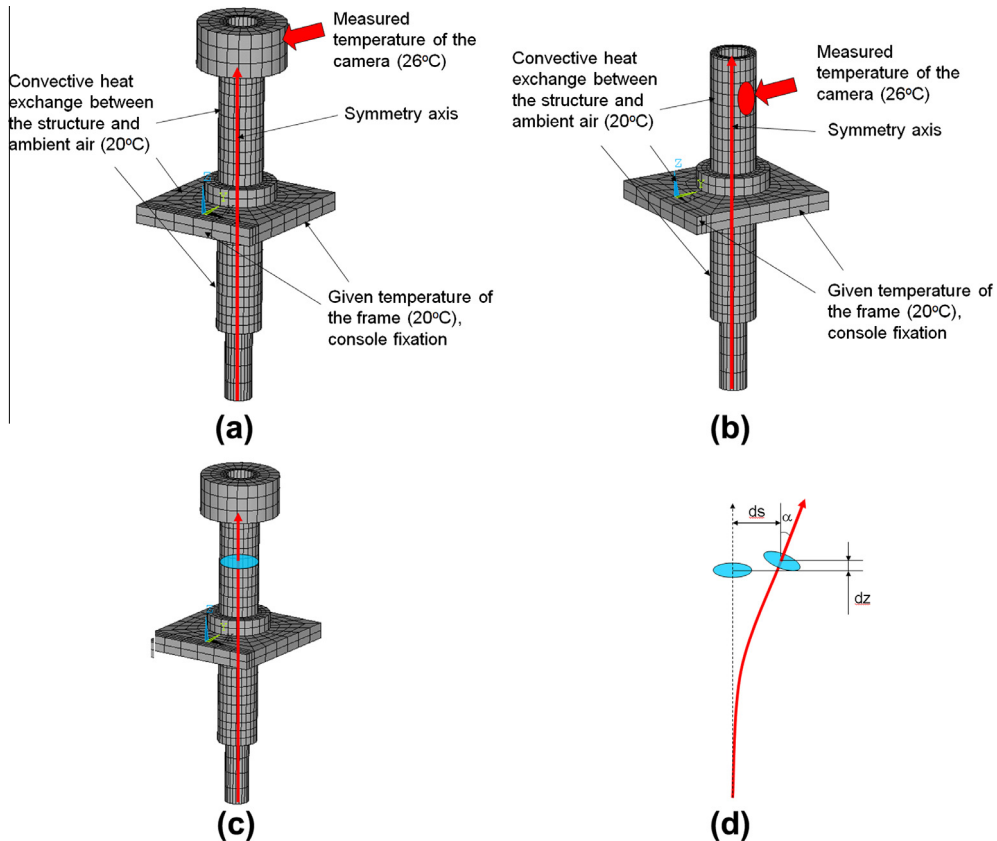


Fig. 1. Model of microscope structure with CCD camera fixed on the symmetry axis (a), CCD camera fixed on the microscope side (b), typical cross-section (c) and displacements under temperature deformations (d).

On the base of Eq. (2) the FE computational model of the microscope and its support structure has been set up as shown in Fig. 1. The model has been implemented in ANSYS finite element software by using elements SOLID70 and SOLID45 for performing the sequentially coupled thermal–mechanical analysis. The model is capable to predict the behaviour of the system under thermal load in case the ambient air temperature is known. It enables us to investigate thermo-mechanical processes in the system and facilitates finding proper structural solutions to reduce the impact of thermal load on the calibration accuracy. Two different constructions have been investigated where the CCD camera is fixed at the top of the microscope structure centred at the symmetry axis (Fig. 1a) and where the CCD camera is fixed at the side of the microscope (Fig. 1b). The warp of the microscope axis due to temperature deformations has been considered as an important pattern of the deformation of the structure, Fig. 1c and d.

In both cases (Fig. 1a and b) we assume that the temperature of the CCD camera is measured and known as 26 °C. The microscope is mounted on the support, which is employed for the 3D positioning of the microscope. We assume that at a certain distance from the microscope tube the temperature of the support is equal to the temperature of the overall structure (~20 °C). At all other surfaces of the structure the convective heat exchange with ambient air (~20 °C) is assumed. The following material constants have been employed: heat conduction coefficients of the microscope tube are 54 W/m K and of the CCD camera and the gaskets 27 W/m K. Surface convection coefficient is 20 W/m K, and heat expansion coefficient is 65×10^{-5} .

Displacements in the structure caused by the calculated temperatures field within the structure are depicted in Fig. 2 in case the CCD camera is situated on the top of the microscope on its symmetry axis. It is important that the raise if the temperature below the support is insignificant in case good thermal contact between the microscope tube and the support is ensured.

The geometrical deviations of the structure in axial and lateral direction are presented in Fig. 3. In this structure axial deviations prevail, which may influence only the focusing of the beam without any essential impact on its position along the scale. The angular deflections of the microscope axis in case of the CCD camera centered on symmetry axis are negligible.

Quite different pattern of the thermo-mechanical deformations is exhibited in case of the CCD camera fixed at the side of the microscope, Fig. 1b. Displacements in the structure caused by the calculated temperatures field within the structure are depicted in Fig. 4, and the geometrical deviations of the cross-section of the microscope tube are presented in Fig. 5. In this case all types of the deviation–deviation of the axial orientation α , defocusing dz and eccentric discrepancy ds are observed. The finite element model should take into account the following physical phenomena:

- heat conduction in ambient air due to its heat conductivity;
- variation if the air temperature caused by the convective heat transfer with the moving air in the vicinity of the comparator structure;

- convective heat transfer between the air and the comparator structure;
- heat conduction within the comparator structure;
- deformations of the comparator structure due to inhomogeneous temperature field within the structure.

The free convective heat transfer is modelled by using the continuity equation, three momentum (Navier–Stokes) laminar flow equations for modelling the free air flow velocities and the convection equation for modelling the heat transfer, all written for volume V of a finite element. The five equations are treated as a PDE system and read as follows:

$$\begin{aligned} \frac{\partial \rho}{\partial t} + \frac{\partial(\rho v_x)}{\partial x} + \frac{\partial(\rho v_y)}{\partial y} + \frac{\partial(\rho v_z)}{\partial z} &= 0 \in V \\ \frac{\partial(\rho v_x)}{\partial t} + \frac{\partial(\rho v_x v_x)}{\partial x} + \frac{\partial(\rho v_x v_y)}{\partial y} + \frac{\partial(\rho v_x v_z)}{\partial z} &= \rho g_x - \frac{\partial p}{\partial x} + \mu \left(\frac{\partial^2 v_x}{\partial x^2} + \frac{\partial^2 v_x}{\partial y^2} + \frac{\partial^2 v_x}{\partial z^2} \right) \in V \\ \frac{\partial(\rho v_y)}{\partial t} + \frac{\partial(\rho v_y v_x)}{\partial x} + \frac{\partial(\rho v_y v_y)}{\partial y} + \frac{\partial(\rho v_y v_z)}{\partial z} &= \rho g_y - \frac{\partial p}{\partial y} + \mu \left(\frac{\partial^2 v_y}{\partial x^2} + \frac{\partial^2 v_y}{\partial y^2} + \frac{\partial^2 v_y}{\partial z^2} \right) \in V \\ \frac{\partial(\rho v_z)}{\partial t} + \frac{\partial(\rho v_z v_x)}{\partial x} + \frac{\partial(\rho v_z v_y)}{\partial y} + \frac{\partial(\rho v_z v_z)}{\partial z} &= \rho g_z - \frac{\partial p}{\partial z} + \mu \left(\frac{\partial^2 v_z}{\partial x^2} + \frac{\partial^2 v_z}{\partial y^2} + \frac{\partial^2 v_z}{\partial z^2} \right) \in V \\ &\lambda \left(\frac{\partial^2 T}{\partial x^2} + \frac{\partial^2 T}{\partial y^2} + \frac{\partial^2 T}{\partial z^2} \right) + b(x, y, z) \\ &= \rho c \frac{\partial T}{\partial t} + \rho c \frac{\partial(T v_x)}{\partial x} + \frac{\partial(T v_y)}{\partial y} + \frac{\partial(T v_z)}{\partial z} \in V \end{aligned} \quad (3)$$

where v_x , v_y , v_z are the components of the velocity vector in the x , y and z directions, respectively, T is temperature, p is pressure, ρ is the mass density, c is the specific heat, λ is the heat conductivity coefficient, $b(x, y, z)$ is employed in order to describe the heat powers (if any) generated within the element volume, (g_x, g_y, g_z) is the vector of the free-fall acceleration.

The free-convection boundary conditions are defined only over the external surface of the surrounding air finite element structure and read as follows

$$T - \tilde{T} = 0; \quad p - \tilde{p} = 0; \quad v_x = v_y = v_z = 0 \in S_{\text{ext}} \quad (4)$$

This means, the surrounding air region should be assumed large enough that the assumed zero boundary conditions do not interfere with the reality.

The zero-velocity boundary conditions are imposed on all surfaces separating the air and the comparator structure as

$$v_x = v_y = v_z = 0 \in S_{a-c} \quad (5)$$

However, pressures and temperatures remain as unknowns on the separating surfaces.

One may notice that in the case of non-moving air $v_x = v_y = v_z = 0$ over all the volume system (2) is simplified to (1). This means that the air is treated as a “solid region”

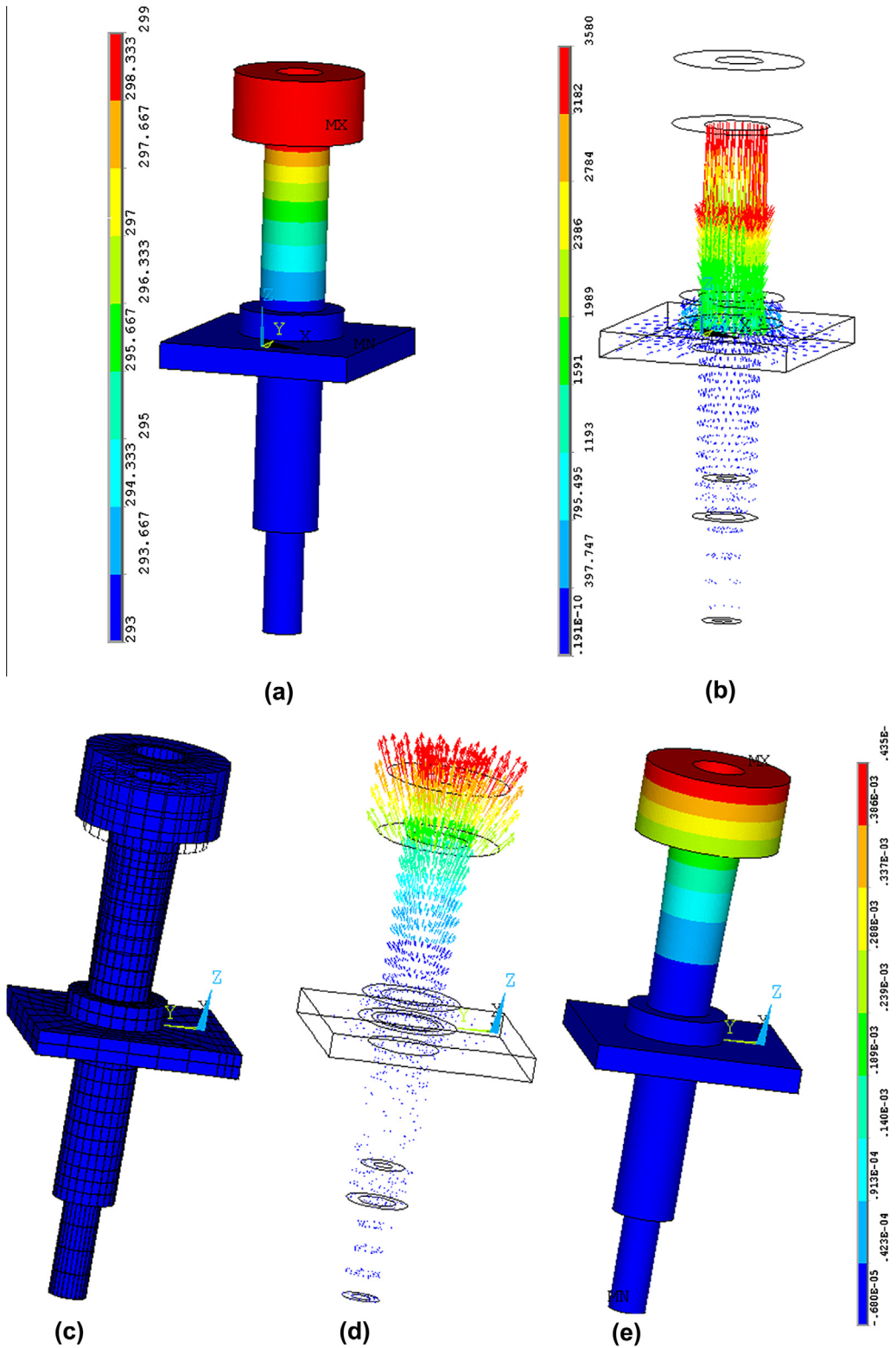


Fig. 2. Calculated temperatures of the microscope structure and its displacements due to temperature deviations (case Fig. 1a): contour plots of the temperatures (a), heat flux density (b), 3D view of the deformed structure (c), vector plot of nodal displacements (d) and contour plot of displacements along Oz axis (e).

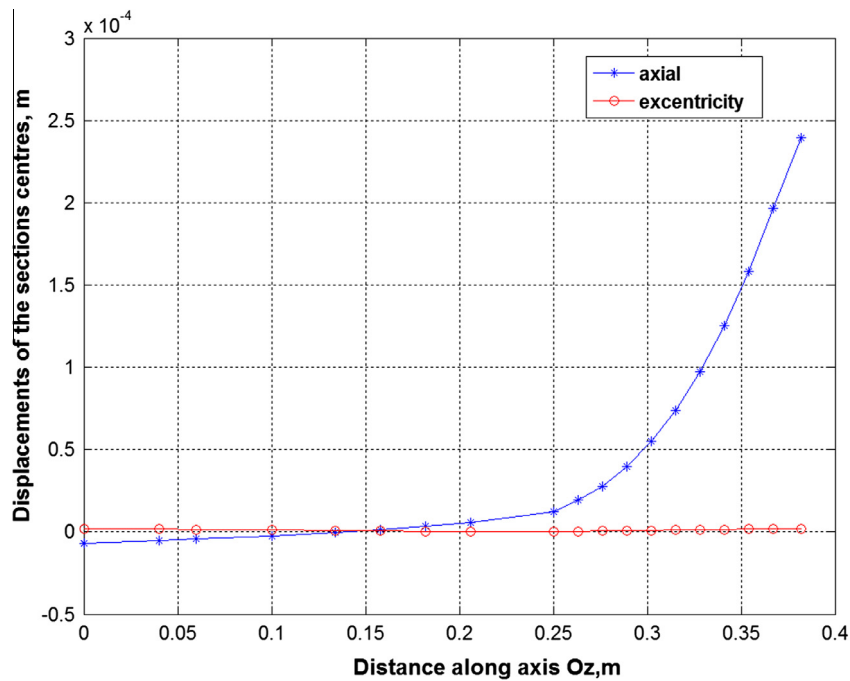


Fig. 3. Axial and lateral displacements of the microscope along the optical axis (case Fig. 1 a).

with heat conduction properties of the air, where only diffusive (i.e. conduction-based) heat transfer takes place.

In ANSYS (FLOTRAN) finite element software the model based on Eq. (3) is referred to as the conjugate heat transfer problem for the solution of which element FLUID142 is employed. In a conjugate heat transfer problem, the flow results depend from density gradients brought about by temperature variations. Most natural convection problems have no externally applied flow sources. Finite elements of the air are based on full system (3), and finite elements of in solid regions (i.e. the structure of the comparator) are based on Eq. (1). In this way the overall investigated combined region of the line scale comparator + surrounding air is presented as a unique FE model. The solution of the model equations provides the air velocities, pressures and temperatures at all points of the model of the air, and only temperatures at points of the comparator structure. After temperatures of all nodes of the comparator structure are obtained, the elements of the comparator structure are replaced to SOLID45 or to SOLID95 solid for performing the sequentially-coupled thermal-mechanical analysis, as described earlier in this section. The obtained results of FE calculations are presented in Figs. 6 and 7.

The most sensitive degrees of freedom for the microscope optics are the two axes of tilt perpendicular to the optical axis, which respectively result in deviations of the focal spot [10]. The influence of a more uniform temperature distribution on the tilt error depends on the type of disturbance, the dimensions of the segment as well as the material properties of the segment. The results of calculations have proven that microscope structure layout with the camera on top is more favourable respectively lateral deviations. The FE model predicted about 1 arcsec tilt of the structure.

Axial thermal expansion of a tube structure due to a temperature gradient around the circumference of the tube causes the tilt error motion. The magnitude of displacement of the focal spot will directly depend on magnification of the objective, focal length of the tube lens and the tilt angle [5].

4. Experimental setup

The FE analysis conducted gave an approximate values and locations of the expected high- and low-temperature zones, along with expected deformations, e.g. at the tip of CCD microscope. Further, detailed experiments on the physical setup were conducted to provide a more accurate characterisation of the thermal profile of the structural components of the comparator and the resultant deformations in free air.

The temperature distribution on the comparator components and in the surrounding air was monitored using PP2 temperature measurement system [11] with max. 22 temperature detectors Pt100. Within the calibration range from 19 °C to 21 °C the measurement uncertainty of the temperature detectors was below 0.022 °C.

In order to determine the distribution of the temperature fields around the microscope camera of the comparator system displayed in Fig. 8a, temperature sensors were arranged in the way, as shown in Fig. 8b, that constant temperature curves (isotherms) could be represented in certain cuts.

To measure the temperature around the microscope camera, 21 sensors were used: four sensors were glued onto the microscope frame, one – onto the flashbulb, one onto the camera, and one onto the camera setting device; the rest of them were laid out in the air.

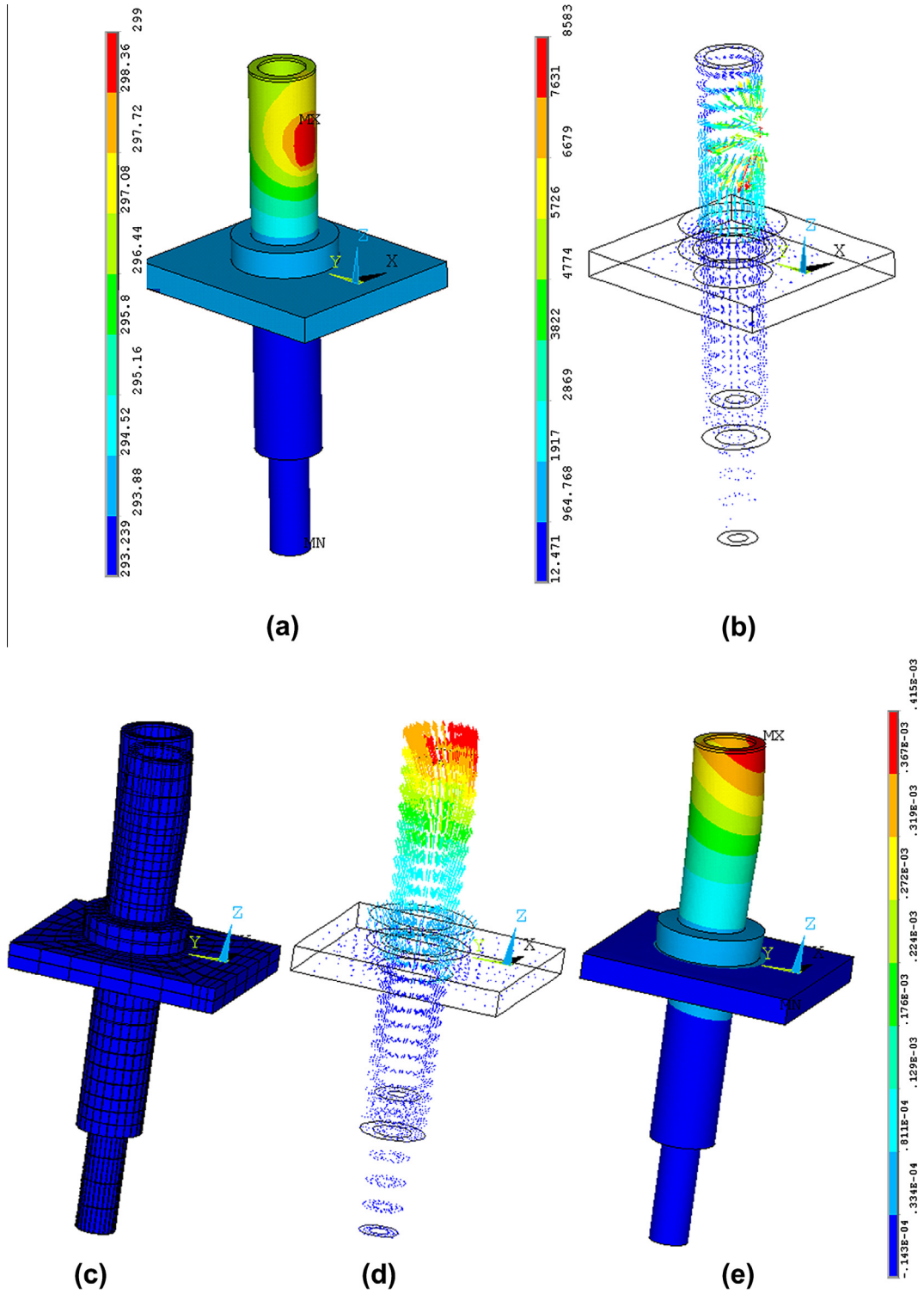


Fig. 4. Calculated temperatures of the microscope structure and its displacements due to temperature deviations (case Fig. 1b): contour plots of the temperatures (a), heat flux density (b), 3D view of the deformed structure (c), vector plot of nodal displacements (d) and contour plot of displacements along Oz axis (e).

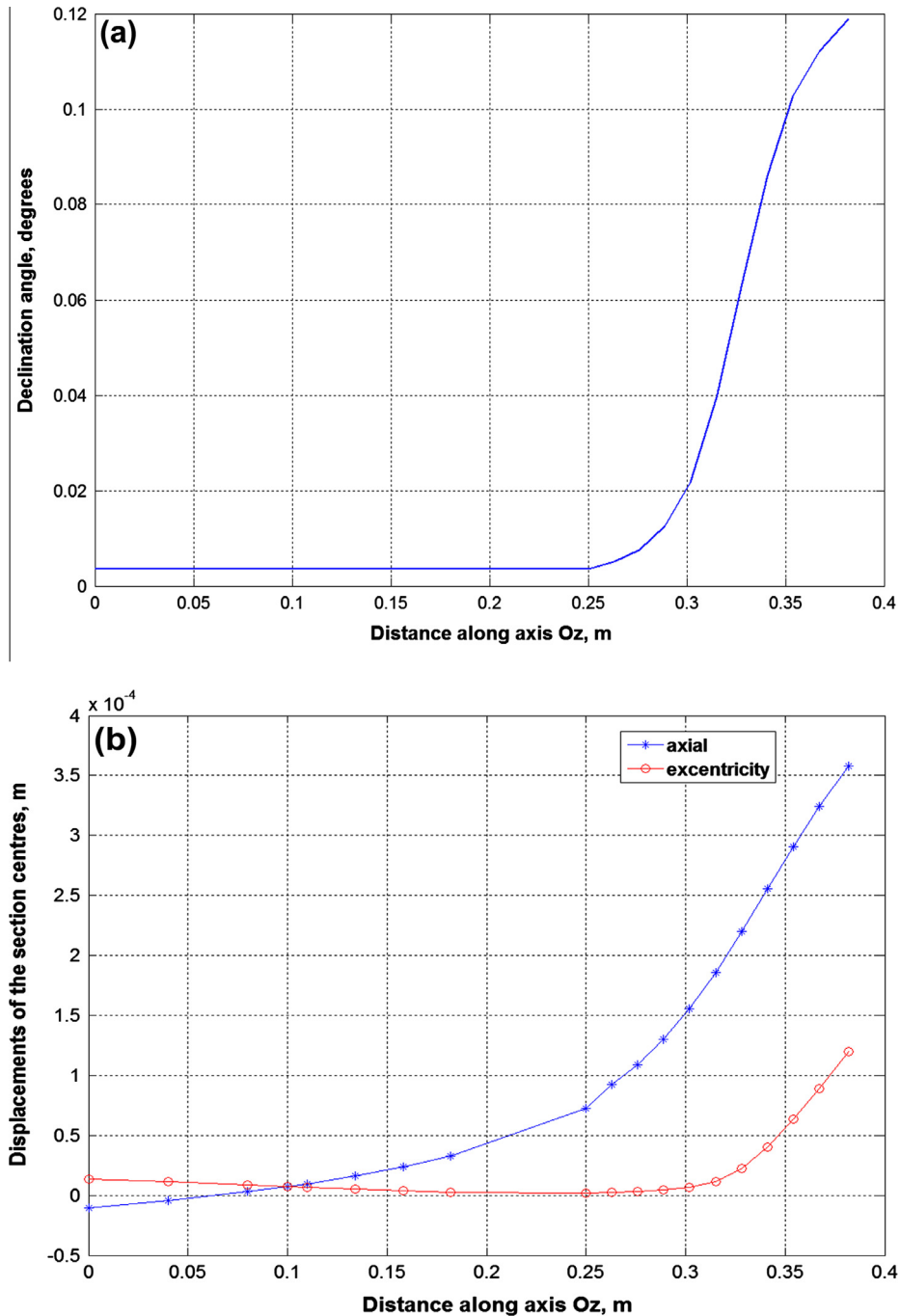


Fig. 5. Microscope axis declination angles (a) and axial and lateral displacements (b) of the points on the microscope optical axis along the optical axis (case Fig. 1b).

Measurements have been basically divided in three phases:

- rest phase when all possible heat sources are switched off for a longer time and temperature of the main comparator components have temperature which is equivalent to one of ambient environment;
- warm up phase, when CCD camera or laser is on;

- steady working phase after the thermal equilibrium is reached between the comparator structure and ambient environment.

Additionally temperature measurements have been performed at the most critical points, i.e. around the scale to be measured as well as at the CCD microscope structure, with a certain time offset before calibration process and

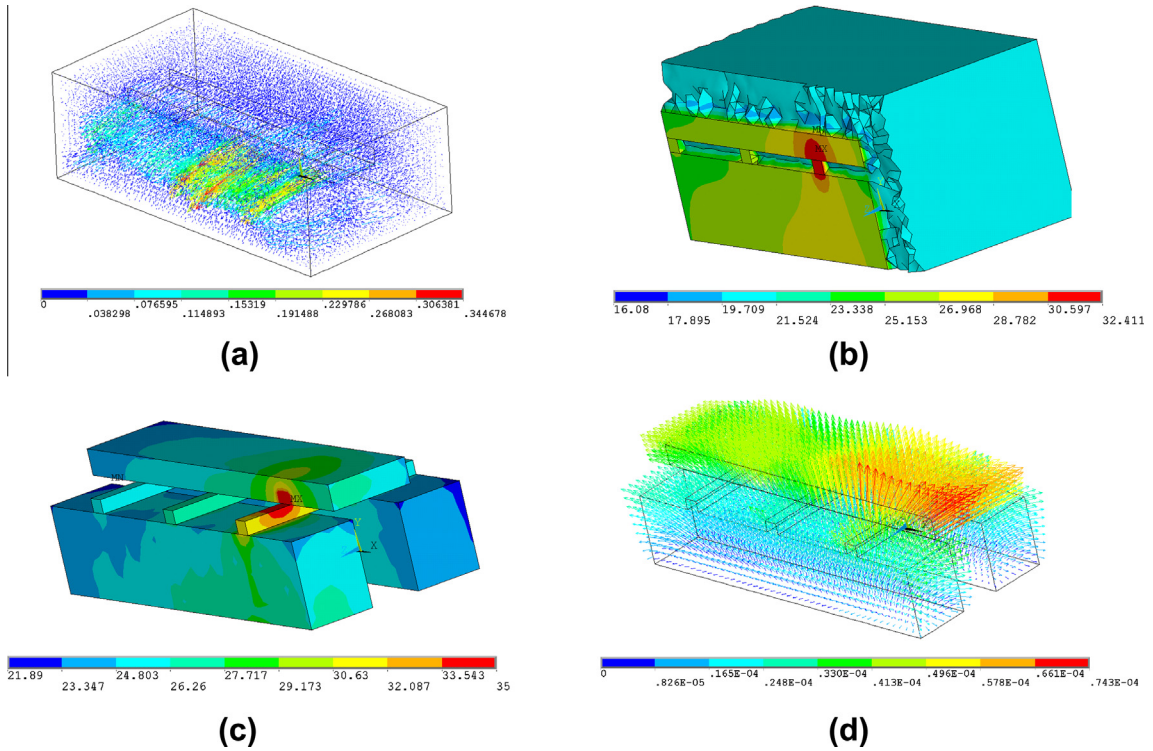


Fig. 6. Results of thermal analysis FE model of the comparator: vector plot of air velocities, temperature distribution over the air-comparator model (b and c), vector plot of mechanical displacements (d).

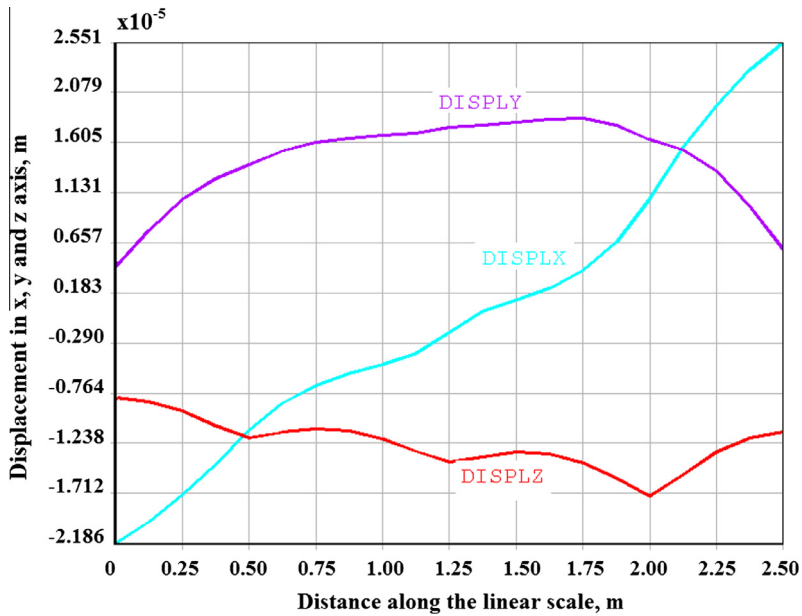


Fig. 7. Mechanical displacements in x, y and z directions along the centre-line of the scale.

during three subsequent calibrations when all devices are operating.

Preceding monitoring of ambient environment of the comparator laboratory has revealed that temperature

variations inside the temperature controlled laboratory can range from +19.75 °C to +20.54 °C. Maximum ambient temperature variations (up to +20.25 °C) have been observed in the calibration zone above the laser. Rejection

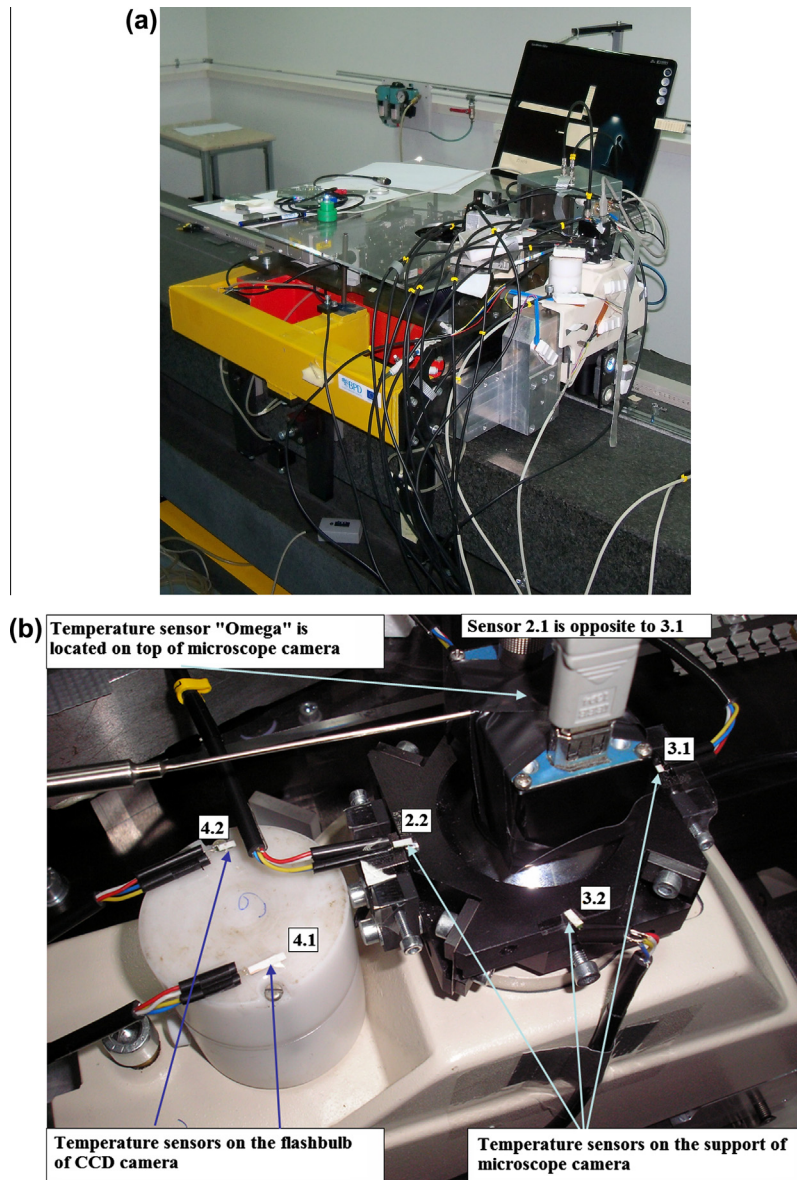


Fig. 8. Layout of the comparator system during temperature measurements (a), distribution of temperature sensors on the optical microscope system (b).

of the most intensive zones of temperature disturbances lead to presumable temperature distribution between $+19.95\text{ }^{\circ}\text{C}$ and $+20.03\text{ }^{\circ}\text{C}$ within the whole room.

Temperature gradient has been estimated with reference to the temperature variations of specific point above the centre of the comparator and the temperature of this point was used for temperature control in the comparator laboratory. Results obtained within one week have been estimated as standard deviation ranging from $0.040\text{ }^{\circ}\text{C}$ during the whole period up to $0.060\text{ }^{\circ}\text{C}$ during the working time.

5. Thermal error measurement

Multiple contact temperature measurements have been conducted (at the top of microscope camera, supporting

mechanism of the optical system and flashbulb of CCD camera) as well as monitoring of ambient thermal fluctuations near the measured scale was performed in order to determine variation of temperature errors in time at CCD cut-off, warming up, and steady operating conditions.

The sensors were placed on CCD microscope structure or at equivalent locations for both evaluation of thermal stability of the optical microscope and monitoring of temperature fields around the system.

The scatter of temperatures around the microscope in a transition phase is depicted in Fig. 9. It clearly manifests temperature inhomogeneity at different locations and shows the speed of transitional processes.

For example sensor 1 represents temperature shift of the support of the optical microscope, sensors 2, 15, 16

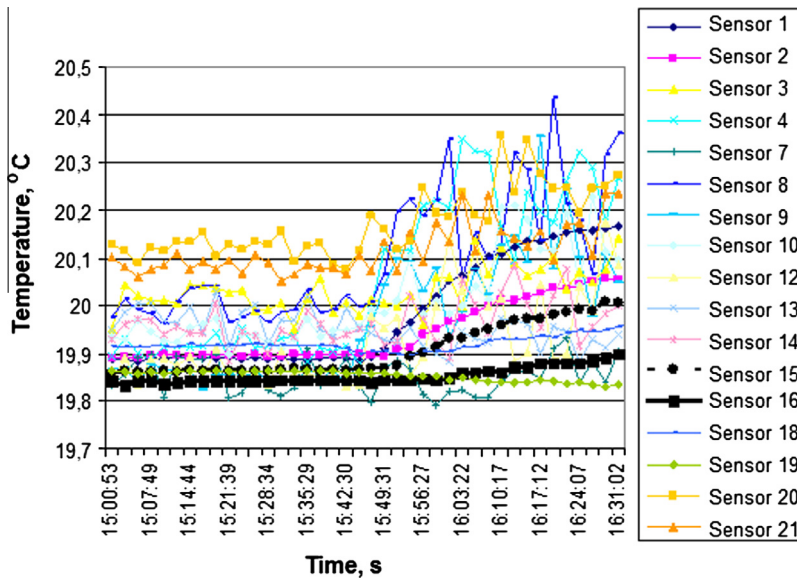


Fig. 9. Temperature variations measured by sensors located on and around the microscope structure.

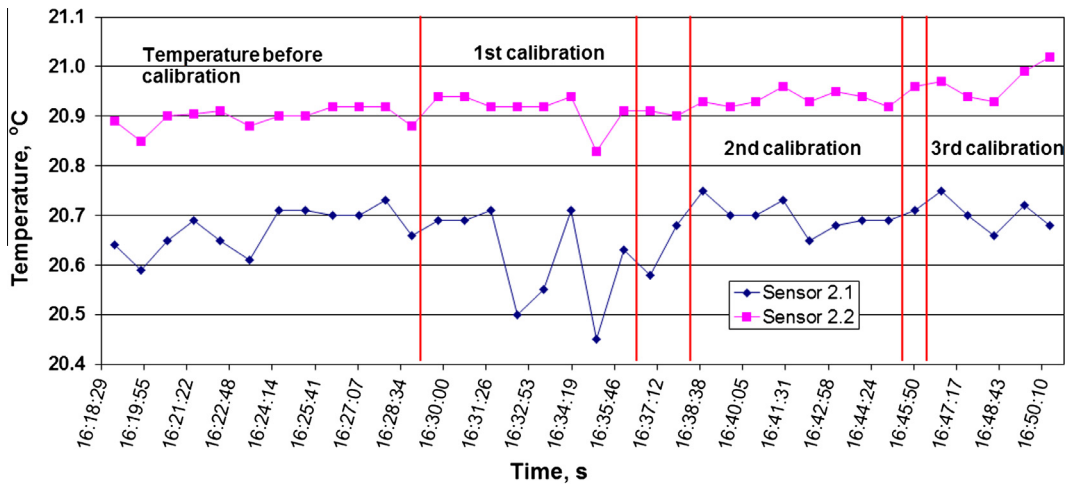


Fig. 10. Temperature deviations at the support of the CCD camera.

and 19 are measuring temperature distributions on microscope housing, apart from the camera. These changes could be approximated by an exponential law similar to one obtained in FE calculations. Although temperature variations on the camera setting device is less significant compared to ones at the top or the flashbulb frame, the above mentioned factors have an influence on the temperature drift up to 0.2 °C that subsequently results in temperature deformations of the camera setting device and contributes to measurement uncertainty budget. Temperature deviations of the support of the camera measured by two sensors (see Fig. 8b) are presented in Fig. 10. Calibration error caused by a thermal CCD camera impact under steady-state calibration conditions is of a random nature, and it cannot be compensated in real-time by numerical compensation techniques.

The ambient air temperature around the calibrated scale has been measured before each calibration and during three subsequent calibrations. Temperature measurement results are depicted in Fig. 11. Temperature variations of 0.1 °C have been observed; they could be influenced by a number of factors such as sources of the increased heat amount in the vicinity of the calibrated scale, and instability of air fluxes in the laboratory. A typical method for improving the positioning accuracy is stabilization of the ambient conditions in the laboratory. However, although having an ideal air conditioning system, by the time the stabilized air reaches the laser beam, it is turbulent and riddled with temperature variations. Despite the stabilized conditions, a variation of tens of mK can be observed as shown in Fig. 12. With a conventional environmental compensation system the amount of variation seen

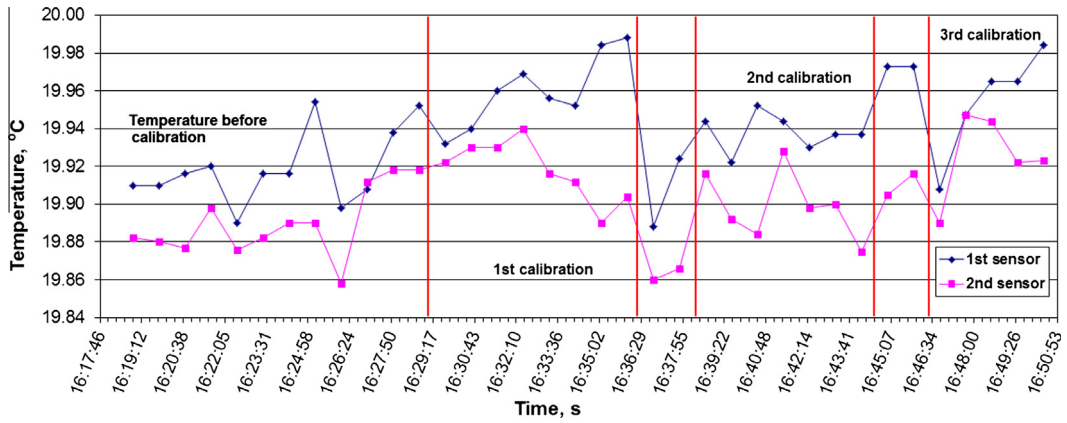


Fig. 11. Temperature variations around the measured scale.

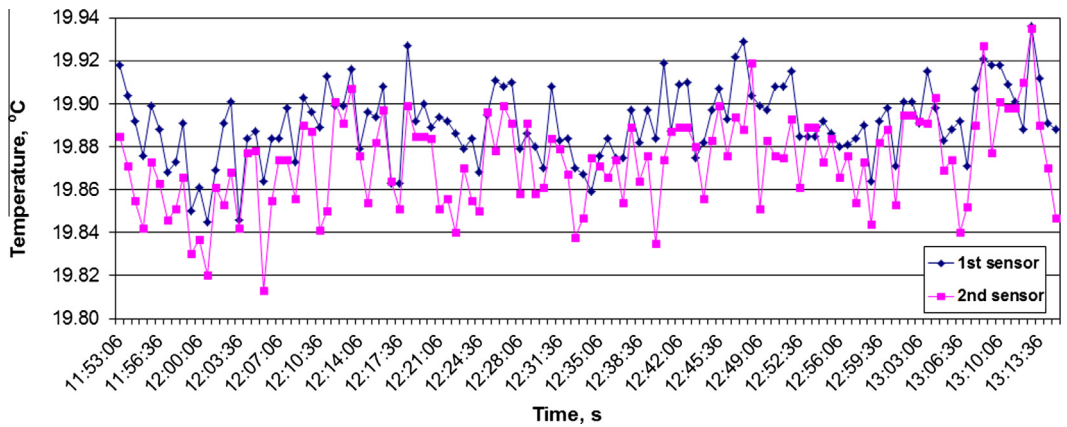


Fig. 12. Temperature variations along the path of laser beam, 600 mm away from the laser.

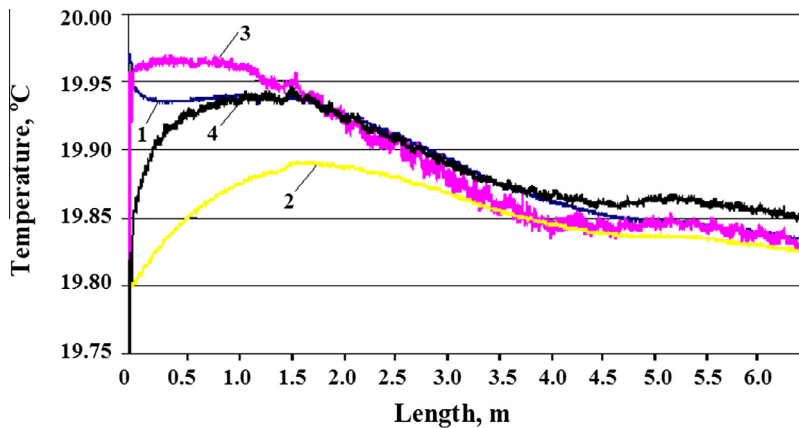


Fig. 13. Temperature gradients in granite base and surrounding ambient air.

in the picture would result in about ± 10 nm positioning error with laser beam path length of 600 mm.

Temperature gradients originated due to thermal inertia of the massive granite base that are affecting the measured scale were analysed too. Measurements have been

performed at different points on the granite table: measurement position near the laser (1st curve) and position, which represents the average temperature of the base (2nd curve). Ambient temperature near these points has been registered too (3rd and 4th curve respectively).

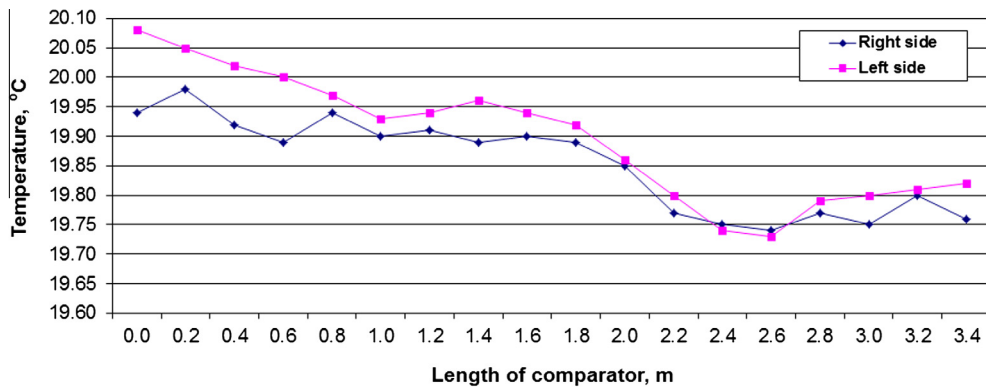


Fig. 14. Temperature distribution on granite base along the working zone.

Experiments were carried out within two days when temperature control system in the laboratory was switched off, and all possible heat sources were eliminated. Measurement results depicted in Fig. 13 clearly reveal that under these conditions temperatures of these specific points practically have been stabilized and uniform during this period. They also indicate the influence and scope of thermal inertia of massive granite base in respect to the temperature variations of ambient environment.

Additionally, an investigation of thermal inhomogeneity of the granite table along the working plane on both sides of the comparator has been accomplished. Measurement points were distributed with spacing of 200 mm. Measurement results are presented in Fig. 14.

The measurement data obtained show that within the measurement range of 3.5 m, temperature at the working plane of granite base can vary up to 0.25 °C on the side which is closer to the outer wall, and up to 0.45 °C on the other side, respectively. Moving away from the laser system temperature in the working plane of the comparator base is decreasing, and these irregularities are to be taken into account while evaluating the effective temperature.

The direct outcome of thermal deformations of the microscope frame structure is line detection errors originated due to geometrical instability of metrology loop. Additionally the measurement error is increasing due to microscope defocusing which leads to reduced quality of line profile images obtained by line detection system. Suppression of high frequency components in the image due to defocusing leads to a certain misrepresentation of the amplitude of optical signal.

Along with the measurements of temperature deviations in the comparator environment the variations of the scale calibration error have been analysed too. Temperature measurements of the microscope structure during subsequent scale calibrations have revealed temperature deviations within 0.6 °C on the top of the camera and up to 0.2 °C on the support mechanism of the microscope resulting in thermal deformations of the microscope frame and determining the scatter of the scale calibration results. The scale of 200 mm length made of Zerodur was used for investigations. Repeated scale measurements under settled ambient conditions (air temperature fluctuations ± 0.05 °C) have shown that due to observed inhomogeneity of

temperature fields around the microscope and temperature gradients in the microscope structure the scale calibration error is increasing. Within multiple calibration experiments conducted an estimated expanded measurement uncertainty amounts to ± 0.23 μm at the 95% probability level ($k = 2$).

Temperature sensors (Pt100) during the experiments were distributed along the working zone of the comparator (every 0.3 m) for measuring of ambient conditions and scale temperature. Readings of the temperature sensors were used for compensation of the laser wavelength variations (according to modified Edlen's equation) and corrections of measurement results for the calibrated scales, particularly for scales up to 3 m long where temperature gradients along the scale are decisive. Temperature measurement software module was realised separately independently from the main control and measurement programme, and these results were used later for thermal error compensation purpose.

Effectiveness of error compensation techniques in dealing with thermally induced errors for improving the accuracy of a machine has been addressed in [1,3,4,12]. The proposed compensation schemes (that aims towards reducing the thermally-induced machining errors) are able to reduce the effect of thermal errors by up to 80%. However, the schemes combining the numerical modelling techniques and experimental investigations are individual and require in-depth analysis of a particular system.

6. Conclusions

The performance of a thermal error compensation system strongly depends on the accuracy and robustness of the thermal error model.

Thermal emission of the heat sources in the machine environment violates standard temperature conditions of calibration space of thermo-constant premises and brings about temperature deformations of the calibrated measure and the comparator elements, thus also causing larger calibration errors.

Measurement errors caused by a thermal inhomogeneity of CCD microscope structure under steady-state calibration conditions is of a random nature and in it cannot be compensated by mathematical methods in real-time.

In order to minimise this calibration error component it is expedient to use the cameras of lower power, symmetric structures made of low thermal expansion materials and to isolate CCD cameras thermally.

References

- [1] R. Ramesh, M.A. Mannan, A.N. Poo, Error compensation in machine tools – a review Part II: thermal errors, *Int. J. Mach. Tools Manuf* 40 (2000) 1257–1284.
- [2] H. Schwenke, W. Knapp, H. Haitjema, A. Weckenmann, R. Schmitt, F. Delbressine, Geometric error measurement and compensation of machines – an update, *CIRP Ann. – Manuf. Technol.* 57 (2008) 660–675.
- [3] M. Weck, P. McKeown, R. Bonse, U. Herbst, Reduction and compensation of thermal error in machine tools, *Ann. CIRP* 44 (2) (1995) 589–598.
- [4] J. Zhu, Robust Thermal Error Modeling and Compensation for CNC Machine Tools, Doctoral dissertation, University Of Michigan, 2008.
- [5] K.C. Wang, P.C. Tseng, K.M. Lin, Thermal error modelling of a machining center using grey system theory and adaptive network-based fuzzy interference system, *JSME Int. J.* 49 (2006) 1–6.
- [6] J.W. Li, W.J. Zhang, G.S. Yang, S.D. Tu, X.B. Chen, Thermal-error modelling for complex physical systems: the-state-of-arts review, *Int. J. Adv. Manuf. Technol.* 42 (2009) 168–179.
- [7] E. Creighton, A. Honegger, A. Tulsian, D. Mukhopadhyay, Analysis of thermal errors in a high-speed micro-milling spindle, *Int. J. Mach. Tools Manuf* 50 (2010) 386–393.
- [8] Michael Bass (Ed.), *Handbook of optics, Fundamentals, Techniques and Design*, Optical Society of America, second ed., vol. I, McGraw-Hill, New York, 1995.
- [9] A.J. Hart, A. Slocum, J. Sutin, Segmented and shielded structures for reduction of thermal expansion-induced tilt errors, *Prec. Eng.* 28 (2004) 443–458.
- [10] A. Jakstas, S. Kausinis, R. Barauskas, A. Kasparaitis, A. Barakauskas, Investigation of dynamics-induced errors of long line scale calibration systems, *Measurement* 44 (2011) 976–987.
- [11] J. Flügge, G. Dai, Design of the temperature measurement and control system at the PTB nanometer comparator, in: *Proc. of the 1st Euspen Topical Conference on Fabrication and Metrology in Nanotechnology*, vol. 2, 2000, pp. 303–309.
- [12] J.P. Kruth, P. Vanherck, C. Van den Bergh, Compensation of static and transient thermal errors on CMMs, *CIRP Ann. – Manuf. Technol.* 50 (2001) 377–380.